Article

Cu/ZSM5-Geopolymer 3D-Printed Monoliths for the NH$_3$-SCR of NO$_x$

Elisabetta Maria Cepollaro [1], **Renata Botti** [2], **Giorgia Franchin** [2], **Luciana Lisi** [1,*], **Paolo Colombo** [2] **and Stefano Cimino** [1]

[1] Istituto di Scienze e Tecnologie per l'Energia e la Mobilità Sostenibili (STEMS), Consiglio Nazionale delle Ricerche (CNR), Via Guglielmo Marconi 4/10, 80125 Napoli, Italy; elisabettamaria.cepollaro@stems.cnr.it (E.M.C.); stefano.cimino@cnr.it (S.C.)

[2] Dipartimento di Ingegneria Industriale, Università degli Studi di Padova, Via Gradenigo, 6/a, 35131 Padova, Italy; renata.botti@unipd.it (R.B.); giorgia.franchin@unipd.it (G.F.); paolo.colombo@unipd.it (P.C.)

* Correspondence: luciana.lisi@cnr.it; Tel.: +39-081-7682279

Abstract: Geopolymer-based monoliths manufactured by direct ink writing, containing up to 60% by weight of presynthesized ZSM5 with low Si/Al ratio, were investigated as structured catalysts for the NH$_3$-SCR of NOx. Copper was introduced as the active metal by ion exchange after a preliminary acid treatment of the monoliths. Monolithic catalysts were characterized by morphological (XRD and SEM), textural (BET and pore size distribution), mechanical (compressive strength), chemical (ICP–MS), redox (H$_2$-TPR) and surface (NH$_3$-TPD) analyses, showing the preservation of Cu-exchanged zeolite features in the composite monoliths. NH$_3$-SCR tests, carried out on both monolithic and powdered samples in the temperature range 70–550 °C, confirmed that composite monoliths provide a very good activity and a high selectivity to N$_2$ over the whole range of temperatures explored due to the hierarchical structure of the materials, in addition to a good mechanical resistance—mostly related to the geopolymer matrix.

1. Introduction

DeNO$_x$ processes for both stationary and mobile sources are mostly based on selective catalytic reduction (SCR) using ammonia as a reducing agent [1]. This technology has been extensively applied to NO$_x$ control in the exhaust products of fossil fuel-fired power plants using V$_2$O$_5$–WO$_3$/TiO$_2$ catalysts [2]. Nevertheless, the application of the SCR technique to the after-treatment of exhaust gas from diesel engines requires catalysts with special features due to a larger operating temperature window. Exhaust gases typically exit at a temperature < 350 °C [3], but the cyclic regeneration taking place into the upstream diesel particulate filter involves gas heating up to or beyond 600 °C [4]. Consequently, catalysts that are active at quite low temperatures but also show a good hydrothermal stability are required.

Zeolites show excellent catalytic properties for NH$_3$-SCR: in particular, ZSM5 has the suitable pore size and acidic character that, coupled to its good thermo-chemical resistance, make this zeolite one of the most used materials in SCR processes when exchanged with suitable active cations [5]. Fe and Cu are the most active metals providing good catalytic performance in a wide operating temperature range [6,7].

Pure zeolite-type technical catalysts are currently limited by the difficulty in producing self-supported monoliths or foams. Zeolite-based structured catalysts are generally produced as a zeolite washcoat deposited on a ceramic substrate, with a consequent low catalyst loading per unit volume of the system and/or risk of loss of the active phase due to poor adhesion and unmatched thermal expansion with the substrate, which are all negative features—especially in mobile applications [8,9].

Self-supported ZSM5 foam monoliths, produced using polyurethane foam templates, were proposed in [10] and successfully tested for the SCR reaction. The foam monoliths showed a good mechanical strength for the highest Si/Al ratio investigated.

The hard diffusion of reactants throughout a microporous structure and the risks of deposition of ammonium nitrates and sulphates in the pores and channels at low operating temperatures in the SCR process [11] suggest the use of hierarchical materials characterized by a large distribution of pore sizes that can improve catalytic performance [12,13].

Geopolymers (GPs) are considered amorphous analogues of zeolites. They are inherently macro/mesoporous materials with a high thermal stability and limited degradation of the structural network up to 800 °C [14]. GPs show good adsorption properties in many applications—typically water purification from organic molecules [15] or dissolved ions [16–19]—but they have been also investigated for SCR reactions both as NH_4- and Cu-GP [20], and Fe-promoted in combination with activated carbon [21]. The possibility of varying their pore architecture in a wide range of values and the close similarity with zeolites concerning ion exchange, make GPs good candidates for the production of composite zeolite–GP materials [15]. For this reason, the integration of the zeolite and geopolymers can take advantage of specific features from both components, such as the high surface area, pore volume, adsorption capacity and catalytic activity of zeolites, and the strength, permeability and support of the geopolymer matrix [22]. These composites have been mostly used as adsorbents, in both gaseous and aqueous systems [23].

The properties of geopolymer–zeolite composites depend on the quantities of zeolites formed in the matrix. The hybrid material can be obtained starting from the GP [24,25] or from the zeolite [26] through suitable hydrothermal treatment, inducing the formation of the other phase, as reviewed in [23]. Unfortunately, the formation of a zeolite fraction is limited to certain structural types, in most cases excluding zeolites with interesting catalytic properties such as ZSM5. Nevertheless, Wang et al. [27] reported hydrothermal formation under high alkalinity synthesis conditions of ZSM5, occurring in aluminosilicate extrudates embedded with β-zeolite which was mostly digested, acting as a nutrient for the growth of ZSM5, forming intra-particle voids and providing a hierarchical porosity. Recently, Li et al. [28] proposed the synthesis of Ce-modified ZSM5 from a geopolymer precursor starting from 5 wt% ZSM5 seeds, although they do not report the final zeolite fraction. Alternatively, the zeolite can be introduced into the GP matrix starting from a pre-formed material. Papa et al. [29] reported the introduction of a commercial Na13X into the GP matrix up to a fraction of 27.3%, obtaining a composite material shaped in the form of a cylindrical foam, casting and curing the zeolite/GP mixture in a closed silicon mold. Those structured foam cylinders display a compressive strength as high as 3 MPa for the composite with the highest zeolite fraction.

Additive manufacturing (AM) enables the fabrication of ceramics with morphologies not achievable using traditional processing technologies [30]. Among all the techniques, direct ink writing (DIW, an extrusion-based approach) permits the ease of design and rapid manufacturing of ceramic-based materials in complicated geometries [31] and, therefore, it is particularly advantageous for lab-scale production and development of structured catalysts [32]. In particular, the architecture of (macro-)porous components can be tailored to simultaneously optimize different properties, such as mechanical strength, permeability, tortuosity and contact time by varying the spatial arrangement of the extruded filaments within the volume of the component [33]. Other AM technologies can also be used to produce catalytic substrates with improved and unique features [34].

The incorporation of 37% commercial ZSM5 into a GP matrix and its final shaping as a monolith by DIW, was first reported in [32] to obtain a structured zeolite catalyst with a hierarchical structure and suitable mechanical properties. In particular, the preliminary washing steps, necessary before ion exchange of GP in order to remove all basic soluble species from the GP matrix [16,32,35,36], were investigated. As for zeolites, the negative charge of the GP network, due to the presence of AlO_4 tetrahedra in the silicate framework, is balanced by extra-framework cations, such as sodium or potassium, which can be

replaced by other cations by ion exchange [20,37,38]. An effective removal of basic alkaline residues must be performed to prevent the inhibition of cation exchange due to a fast precipitation of metal hydroxide.

In this work, we set out to further investigate the synthesis and catalytic performance in the NH$_3$-SCR of NO$_x$ of composite zeolite geopolymer monoliths manufactured by DIW and containing up to 60 wt% ZSM5. The chemical, physical and mechanical properties of the composite monoliths were investigated in detail to validate their use as catalysts for mobile applications.

2. Results and Discussion

2.1. Catalyst Characterization

SEM images of a GP monolith and of the two GP–Z(x) monoliths are shown in Figure 1, where the deposition of continuous filaments with regular diameters following a 0–90° sequential build-up, creating a 3D network, was well visible for all samples. The diameters of filaments ranged from 845 to 880 μm, slightly increasing with zeolite load, consistent with the diameter of the conical nozzle used for printing. The inner section of the GP monolith showed the significant presence of some large pores with dimensions of some tens of microns, attributable to air trapped during the preparation of the ink, which tended to disappear in the composite materials that possess a denser and more homogeneous structure. Images at higher magnification confirmed the absence of needle-like particles associated with residual sodium compounds in all acid-treated samples and showed roughly rounded particles that were generally larger for the pure GP in comparison to the GP–Z composite monoliths.
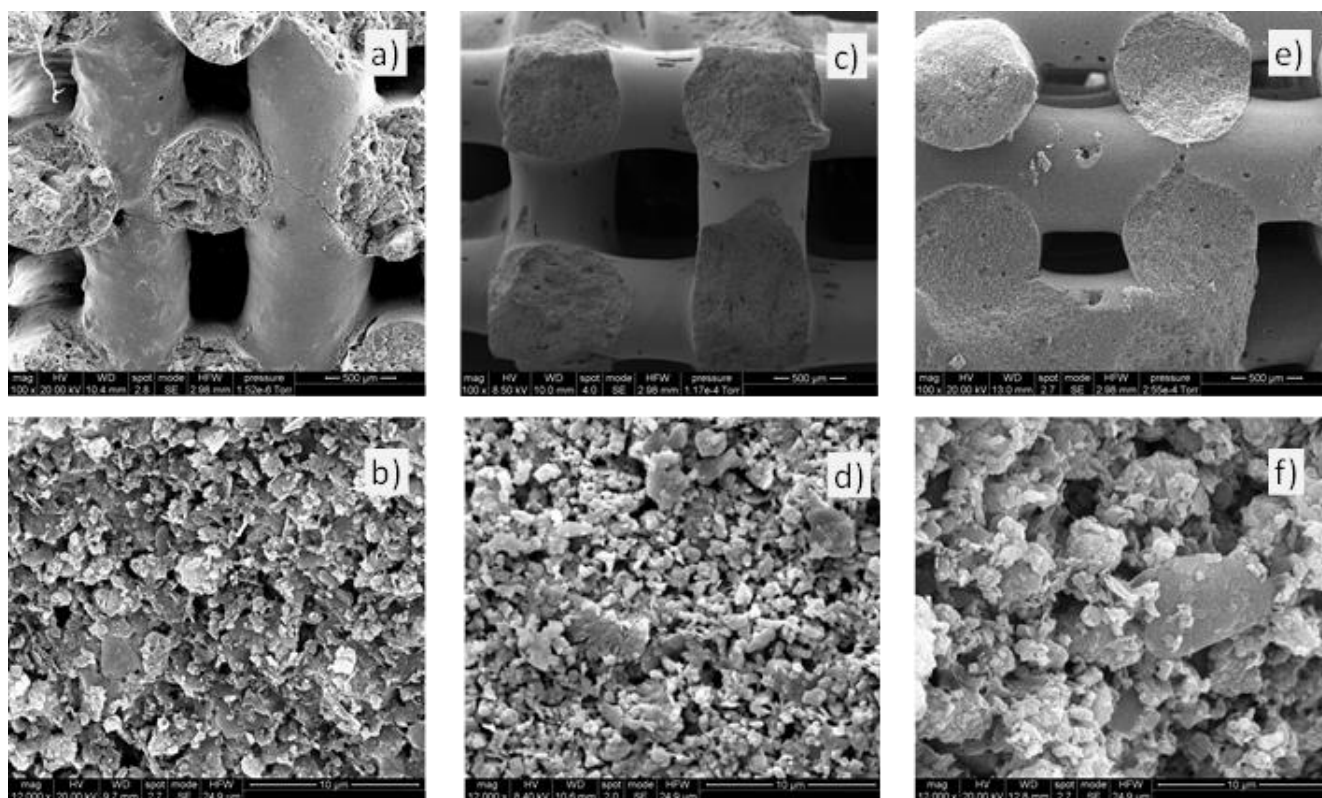
Figure 1. SEM images of the cross-section of the struts of acid-treated GP (**a**,**b**), GP–Z(37) (**c**,**d**) (adapted from [32]) and GP–Z(60) (**e**,**f**) monoliths.

The compressive strength of GP–Z(37) and GP–Z(60) monoliths after the acid treatment was 1.02 ± 0.2 and 0.31 ± 0.15 MPa, respectively: the statistical error is associated to the number of specimens tested (>10 for each composition), some of which can show

structural defects. For comparison purposes, a pure self-supported ZSM5 zeolite monolith foam previously prepared by hydrothermal synthesis with a polyurethane foam template revealed a compressive strength equal to 0.31 MPa [10], that was high enough to stand extensive SCR testing in lab scale reactor. These values are lower than that measured for pure GP monoliths without zeolite that weren't preliminarily treated with acid solution, which was as high as 5.23 ± 0.87 MPa [17]. As expected, the mechanical resistance decreased by increasing the zeolite fraction in the composites, due to the reduction in the amount of GP matrix as well as the disruption of its continuity. A depolymerization of the GP network caused by the acid attack can further decrease the mechanical strength of the monoliths [39].

Figure 2 shows the XRD patterns of the original ZSM5 and GP materials as well as those of the composite monoliths. The higher contribution of the typical ZSM5 signals up to 25° was easily detectable for Cu/GP–Z(60). The amorphous halo centered at 27–29°, typical of the geopolimeric matrix [40], is evident in both fresh GP–Z samples (not shown), whereas it is significantly reduced in the Cu-exchanged samples, mainly due to the preliminary acid treatment which eliminates (part of) the sodium from the geopolymer matrix by ion exchange, partially degrades the geopolymer network (see later), and dissolves the alkaline compounds present on the surface. The removal of these compounds, which can be attributed to the formation of sodium carbonate by reaction with atmospheric CO_2, was also consistent with the disappearance of the needle-like structure observed by SEM analysis, previously reported in [32]. However, the acid treatment did not affect the crystalline structure of the zeolite [32], as confirmed by the XRD patterns of Cu-exchanged materials. No other signals assignable to different zeolite-like phases were detected, thus excluding the possible zeolitization of the GP matrix—different to what was reported when zeolites such as 13X were introduced as a matrix filler [29].
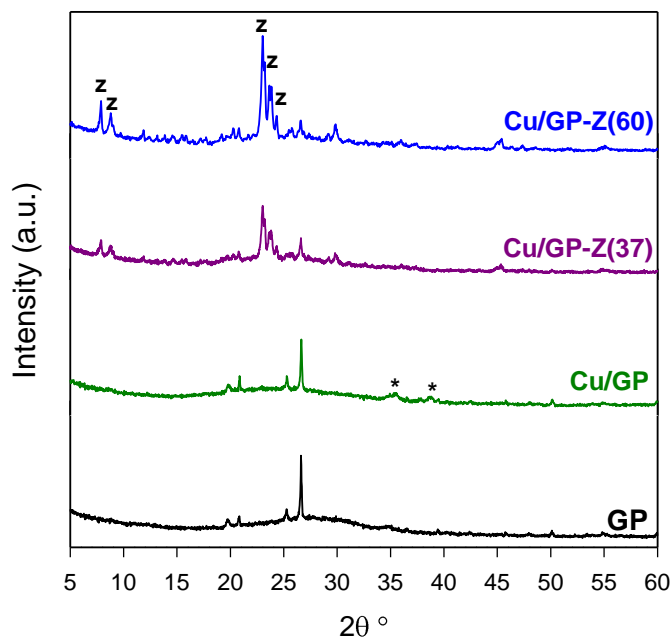
Figure 2. XRD patterns of as synthesized GP and Cu/GP–Z(x) monolith catalysts. Legend: z = ZSM5; * = CuO.

No signals associable to copper oxide were detected in the composite samples, whereas weak signals at 35.5 and 38.7°, attributed to CuO, appeared in the XRD pattern of the Cu/GP monolith, suggesting that some oxide segregation occurred at the GP surface.

Table 1 reports the actual copper load (measured by ICP–MS) in the Cu-exchanged pure and composite geopolymer/zeolite materials. The actual amount of copper in the ZSM5 powder was 3.2 wt%, corresponding to ca 90% of the total cation exchange capacity

(CEC = 0.62 mmol/g for bivalent copper cation), evaluated on the basis of the actual Si/Al ratio in the zeolite.

Table 1. Copper content (by ICP–MS), fractional cation exchange capacity, BET specific surface area, micropore and total pore volumes for Cu-exchanged composite monoliths and their acid-treated precursors compared with pure Cu/GP and Cu/Z (powder).

Sample		Cu Load wt%	Exchange Capacity %	S_{BET} $m^2\ g^{-1}$	V_{micro} $cm^3\ g^{-1}$	V_{tot} $cm^3\ g^{-1}$
H-ZSM5		-		430	0.17	0.25
Cu/Z		3.2	90	415	0.16	0.24
GP–Z(60)	Acid-treated	-		264	0.11	0.17
	Cu-exchanged	2.9		253	0.11	0.19
GP–Z(37)	Acid-treated	-		133	0.05	0.14
	Cu-exchanged	1.5		122	0.04	0.11
GP		-		11	-	0.13
Cu/GP		3.0	20	27	-	0.18

Considering an Al content of 5 mmol/g (dry basis) for the pure GP, its theorethical copper exchange capacity should be as high as 2.5 mmol Cu/g [41], but the actual amount introduced in the monolith by cation exchange was much lower, accounting for ca 20% of the total CEC. This could be caused by the hydrolytic degradation of the Si–O–Al framework [35] which could be the consequence of the electrophilic attack by acid protons on polymeric Si–O–Al bonds, resulting in the ejection of tetrahedral aluminum from the aluminosilicate framework [42,43] and consequent formation of separate domains of SiO_2 and Al_2O_3.

Composite monoliths displayed a copper content that was lower than expected from the linear combination of the values for the corresponding pure materials, and increased along with the zeolite fraction in the monolith. This suggests that the metal was mostly located in the ZSM5 crystals and ion exchange was not precluded by the GP matrix. It is worth mentioning that previous studies have indicated that the ion exchange method for structured (honeycomb) ZSM5 catalysts is less effective than for powder samples, with a double-exchange proceess achieving only ca half the theoretical CEC [10], even in the absence of any other component such as the GP matrix.

Figure 3a reports the N_2 adsorption isotherms at 77 K for Cu-exchanged monoliths, compared with that of the pure Cu/Z powder, showing the typical type I isotherm of microporous solids. The shape of the isotherms was largely preserved in the composite materials, although a clear reduction in N_2 adsorption capacity was observed due to the poor contribution of the GP. Indeed, the Cu/GP monolith showed a predominant meso-porosity (type IV isotherm with a H3 hysteresis loop between adsorption and desorption branches) that was also reported for GP with Si/Al = 1.2 [29], and was further accompaneid by some macroporosity. Table 1 reports the values of BET surface area, micro- and total pore volumes for composite monoliths after acid pre-treatment and after Cu-exchange, compared with the values of the pure Cu/Z and Cu/GP. The commercial ZSM5 after the preliminary deammoniation had a surface area of 430 $m^2\ g^{-1}$ and a total porosity equal to 0.25 $cm^3\ g^{-1}$. Copper exchange induced only a slight decrease in both figures. In contrast, the Cu/GP monolith showed a lower specific surface area value of around 27 $m^2\ g^{-1}$, which was somehow enhanced by the removal of alkaline residues upon preliminary acid pre-treatment and Cu exchange steps [32]; the characteristic dimension of mesopores in the Cu/GP monolith was around 50 Å. Therefore, the BET surface area of the composite samples increased with the zeolite load, and the final Cu-exchange step had only a weak impact on the textural properties of the monoliths, as also observed for the pure Cu/Z sample. Significantly, the BET values of the Cu-exchanged monoliths corresponded well to those expected on the basis of the zeolite and GP contents, especially for the Cu/GP–Z(60) sample. This indicates that the structural properties of the starting materials were mostly preserved upon slurry preparation and its subsequent DIW, giving rise to composite

monoliths with hierarchical textural features, as shown by the pore volume distribution analysis presented in Figure 3b for the exemplificative case of the Cu/GP–Z(37) sample. Papa et al. [29] reported lower values of specific surface area for their composite GP-13X foam composites, likely due to the lower fraction of zeolite in the material, but also a higher pore volume, which reflects the larger microporosity of 13X compared to ZSM5.
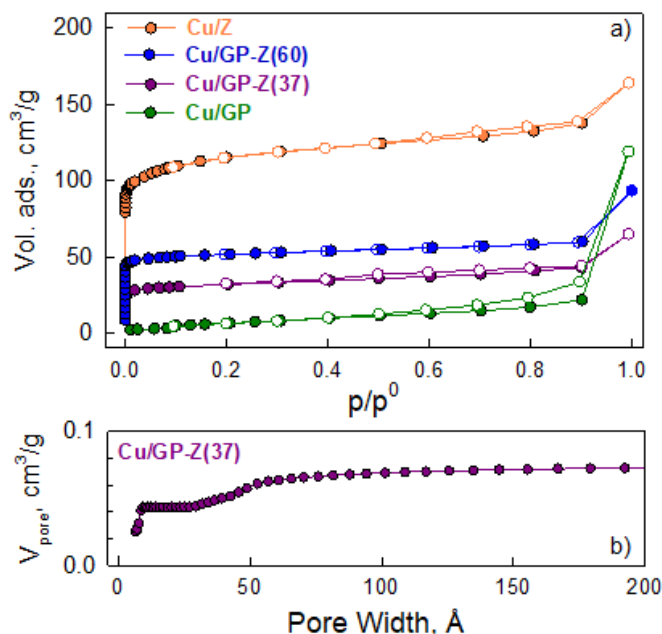

Figure 3. (**a**) N_2 adsorption/desorption isotherms at 77 K over pure Cu/GP and composite Cu/GP–Z(x) monoliths and reference Cu/Z powder; (**b**) Cumulative pore volume as a function of the characteristic pore width for the Cu/GP–Z(37) monolith.

Figure 4 and Table 2 present the results of the H_2 TPR analysis on the two Cu-exchanged monoliths compared with that of Cu/GP and Cu/Z. The overall H_2 consumption corresponds to the complete reduction of Cu content in each sample from +2 to 0. After instrument calibration with a bulk CuO standard, it was verified that the measured H_2 uptakes agreed within ±10% to those expected from the actual metal loading in the samples measured by ICP–MS (Table 2).
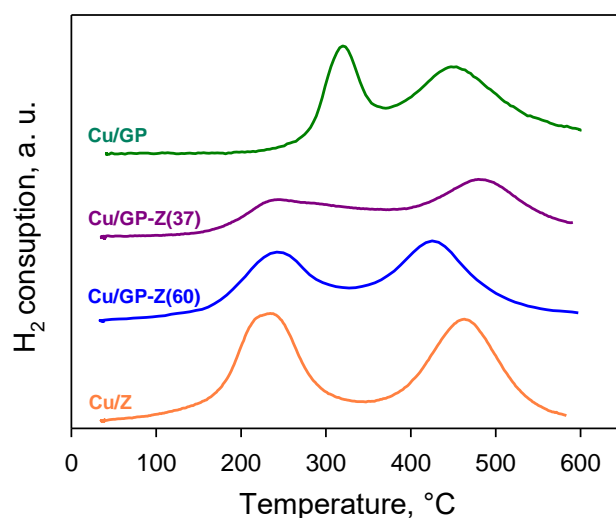

Figure 4. H_2 TPR profiles for pure Cu/GP and composite Cu/GP–Z(x) monoliths and reference Cu/Z powder.

Table 2. Summary of the results for H_2-TPR, and NH_3-TPD (after NH_3 adsorption (@100 °C) tests on Cu/GP and composite Cu/GP–Z(x) monoliths and pure Cu/Z catalyst.

	TPR			TPD
Sample	**H_2/Cu**	**Temperature (°C)**		**Desorbed NH_3**
	mol/mol	**Peak 1**	**Peak 2**	**mmol g^{-1}**
Cu/Z	1.08	239	460	1.17
Cu/GP–Z(60)	0.95	242	436	0.69
Cu/GP–Z(37)	1.04	238	477	0.31
Cu/GP	0.97	320	453	-

It is reported that copper, as an exchanged cation in the ZSM5 framework, is reduced via two subsequent steps corresponding to the reduction from the oxidation state +2 to +1 and then to 0 [8]. Accordingly, the TPR trace of Cu/Z showed two signals with roughly the same area that peaked at ca 230 and 460 °C, respectively. It is worth noting that an asymmetric distribution of peak areas is associated to the additional presence of copper with a different nature, as observed for Cu/ZSM5 on cordierite [8]. Cu/GP also gave two main peaks of similar area centred at 320 and 450 °C, respectively. However, the higher (ca 90 °C) temperature required for the first reduction event of Cu/GP indicates a lower reducibility of the metal and, in agreement with XRD data, it confirms the possible formation of segregated CuO nanoparticles when Cu-exchange is performed on acid-treated GP monoliths.

The shape as well as the characteristic reduction temperatures of the TPR profiles for the composite Cu/GP–Z monoliths were rather similar to those recorded for the Cu/Z sample; in particular, the absence of a reduction event at around 320 °C indicates that the GP matrix in the composite materials gives a modest (if any) contribution and, above all, does not preclude the exchange capacity of the zeolite fraction in the preformed monoliths. Most of the copper content in composite monoliths appears located at the zeolite exchange sites rather than segregated as copper oxide, as in the case of the pure GP monolith. This is the reason why the actual copper loaded in the composite materials decreased along with the zeolite fraction in the monoliths.

The adsorption of ammonia is of paramount importance for the SCR reaction because it is deeply involved in the reaction mechanism. In particular, it has been reported that in addition to NH_3 coordinated to Cu^{2+} ions, active in the SCR reaction, NH_4^+ ions formed on Brønsted acid sites are also necessary—representing an ammonia buffer [28]. The NH_3 adsorption capacity of the catalysts was measured on grinded Cu-exchanged monoliths as well as on mechanical mixtures of pure materials, in order to investigate the effect of the interaction between ZSM5 and GP on the surface acidity of the catalysts. In line with literature data [44,45], the TPD profile of pure Cu/Z (Figure 5) showed a main composite peak with a maximum at about 190 °C, accompanied by poorly resolved shoulders at 260 and 340 °C, which can be assigned to the weak, moderate and strong acid sites, respectively. A further signal between 450 and 600 °C, typical of the pristine H-ZSM5, was largely reduced due to the high copper exchange ratio achieved in our Cu/Z sample [44].

The Cu/GP sample showed a rather flat TPD profile, suggesting that this sample had a negligible ammonia adsorption capacity, in contrast with Li et al. [28], who evaluated an adsorption capacity of 1.75 mmol/g, whereas Saha et al. [46] calculated a capacity as high as 2.14 mmol/g for metakaolin-based geopolymers either in H- or alkaline- form. This is possibly caused by the residual presence of basic compounds on the surface of the Cu/GP sample. Accordingly, TPD profiles of composite materials showed an increasing intensity along with increases in zeolite content. In particular, the total amount of NH_3 released during the TPD by Cu/GP–Z(60) roughly scaled with its zeolite content (Table 2), and the shape of the corresponding TPD trace was rather similar to the reference Cu/Z material. However, the larger GP content in the Cu/GP–Z(37) composite seemed to affect

the acid character of the zeolite fraction, particularly by reducing the number of strong acid sites capable of releasing ammonia above 320 °C. Furthermore, TPD profiles recorded for mechanical mixtures of pure Cu/Z and Cu/GP materials (Figure 5) showed similar qualitative features, but lower amounts of NH_3 desorption with respect to their composite monolith counterparts; this suggests that the intimate contact between the GP and ZSM5 phases established during the preparation of monoliths can favour the elimination of alkaline residues from the GP matrix.
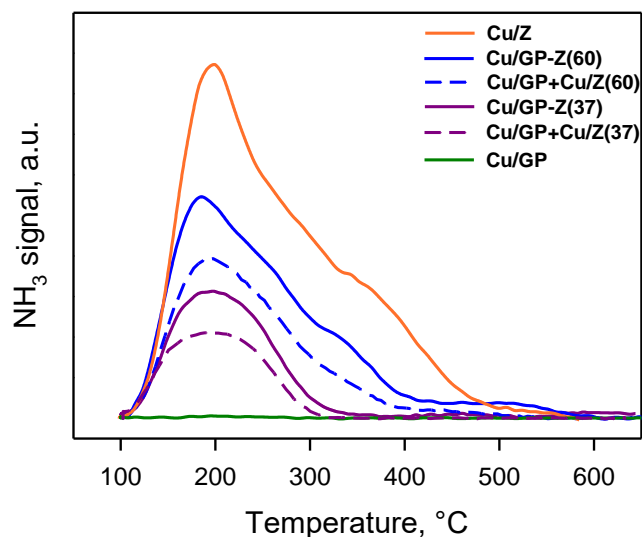

Figure 5. NH_3-TPD profiles for pure Cu/GP and composite Cu/GP–Z(x) monoliths and reference pure Cu/Z, or in mechanical mixtures with pure Cu/GP with identical nominal composition as monoliths.

2.2. NH_3-SCR Tests

NO and NH_3 conversions, N_2O formation and N_2 selectivity measured during the NH_3-SCR tests on monolith catalysts are reported in Figure 6a–d as a function of the reaction temperature. A blank run using an "as-prepared" GP monolith, i.e., without performing any acid pre-treatment and subsequent copper exchange, was carried out in order to show that the SCR reaction does not take place in the absence of copper; ammonia oxidation occurs only at T > 350 °C (Figure 6b), likely homogeneously, leading to the formation of N_2O, NO_2 and, supposedly, N_2—being NO production negligible (Figure 6a).

Copper deposition on the GP monolith provided a detectable catalytic activity. Both NO and NH_3 started to be converted at temperatures as low as 200 °C (Figure 6a,b). A remarkable effect of the introduction of copper on SCR performance was also reported in [20] for NH_4Cu geopolymers. Similarly, it has been reported that the introduction of active iron in geopolymer/active carbon composites strongly improved SCR performance [21]. In agreement with Sazama et al. [20], ammonia oxidation took place over the whole range of temperatures in addition to the SCR reaction, as shown by the larger NH_3 conversion compared to that of NO. NO conversion achieved a maximum at about 250 °C; thereafter, it declined and eventually reached negative values for temperatures above 350 °C. This clearly indicates that NO is one of the products of ammonia oxidation (prevailing at high T) and is formed together with some N_2O (Figure 6c), causing a progressive decline of N_2 selectivity with increasing temperature (Figure 6d).
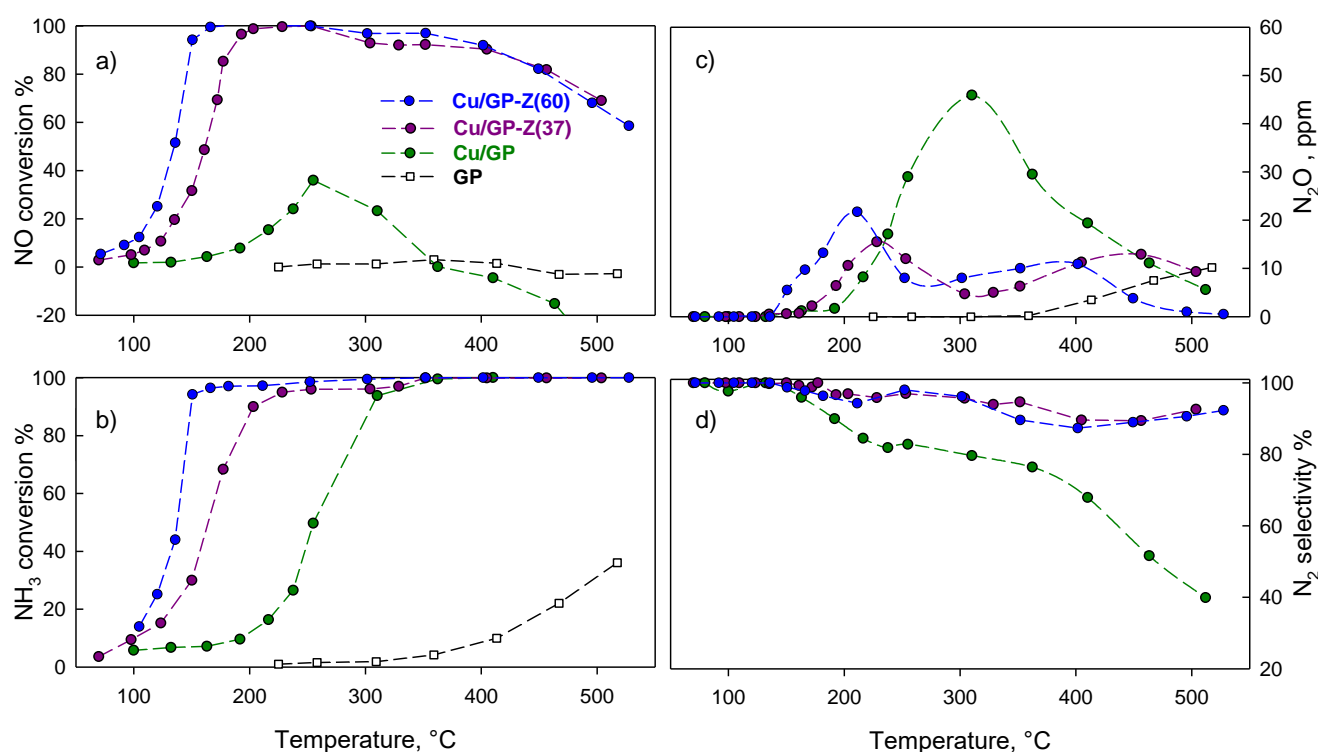
Figure 6. NO (**a**) and NH_3 (**b**) conversion, N_2O production (**c**) and N_2 selectivity (**d**) as a function of the reaction temperature during the NH_3-SCR of NO over GP and Cu/GP-Z(x) exchanged monoliths.

The introduction of ZSM5 into the GP matrix dramatically changed its catalytic behavior. NO conversion approached 100% at about 200 °C for Cu/GP–Z(37) and at as low as 150 °C for Cu/GP–Z(60) (Figure 6a). NO conversion started to decrease for both monoliths above 250 °C due to the simultaneous oxidation of ammonia. Nevertheless, both ZSM5-containing monoliths provided a high value of selectivity to N_2, which stayed close to 100% up to about 300 °C—slowly decreasing beyond this temperature, but keeping values above 90% over the whole range of temperatures explored (Figure 6d). N_2O formation over composite monoliths was very limited (Figure 6c), reaching maximum levels below 20ppmv at temperatures of around 220 °C, in good agreement with previous data reported for self supported Cu-ZSM5 foam catalysts [10].

Catalytic tests were also repeated at a shorter contact time using ground and sieved composite monoliths as well as mechanical mixturess of pure components with the same nominal composition (Table 3).

Table 3. Apparent activation energy (E_a) and first-order kinetic constant values at 150 °C (k_w, k_{wz}: per unit mass of catalyst or zeolite fraction, respectively) for the NO removal rate by NH_3-SCR on composite Cu/GP–Z(x) and reference catalysts calculated from conversion data collected under the specified experimental conditions.

Catalyst	Form	F/W_{cat} $dm^3 g_{cat}^{-1} h^{-1}$	E_a $kJ\ mol^{-1}$	k_w (150 °C) $cm^3 g_{cat}^{-1} s^{-1}$	k_{wz} (150 °C) $cm^3 g_{zeolite}^{-1} s^{-1}$
Cu/Z	Powder	200	64.8	20	20
Cu/Z Foam [a]	Monolith	40	74.6	3.4	3.4
Cu/GP–Z(60)	Monolith	13	65.1	6.0	10
Cu/GP–Z(37)	Monolith	14	68.1	2.8	7.6
Cu/GP–Z(37)	Powder	200	68.1	2.8	7.6
Cu/GP+Cu/Z(37) [b]	Powder	200	65.0	1.7	4.6
Cu/GP	Monolith	15	48.8	0.2	-

[a] adapted from ref. [10]. [b] mechanical mixture: 63 wt%. ground Cu/GP monolith + 37 wt%. Cu/Z powder.

Data reported in Figure 7 for the case of Cu/GP–Z(37) indicated that both NO conversion and N_2 selctivity were sistematically higher for the ground monolith rather that for its mechanical mixture counterpart, suggesting that the negative contribution of Cu/GP to the overall catalytic behaviour is still detectable when the two materials are simply mixed, whereas the catalytic features of Cu/Z prevail when a more intimate contact is estabilshed during the production and printing of the composite monolith catalysts.
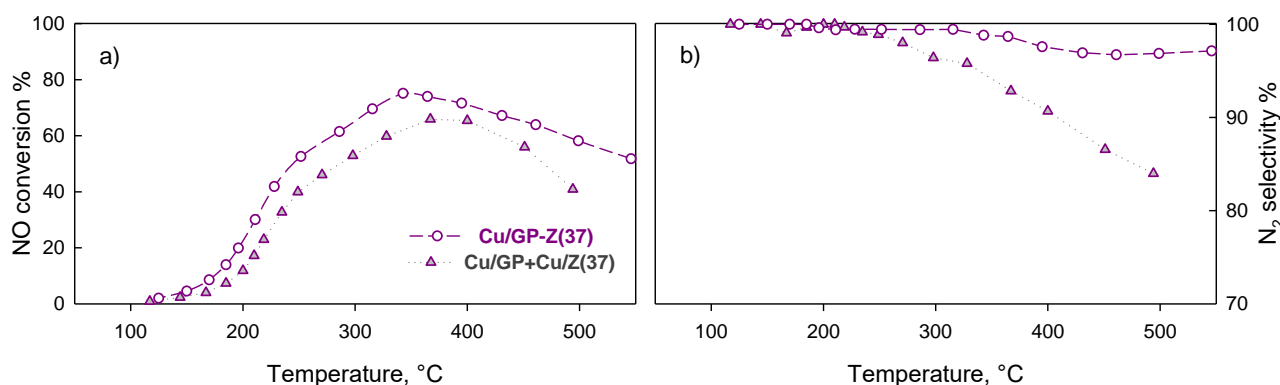

Figure 7. (**a**) NO conversion and (**b**) N_2 selectivity as a function of the reaction temperature during the NH_3-SCR of NO on a powdered Cu/GP–Z(37) sample and on a mechanical mixture of pure Cu/GP and Cu/Z powders with identical nominal composition.

All catalytic results were elaborated on the basis of integral reactor conversion data, assuming an ideal isothermal plug flow behaviour and a first-order dependency on NO concentration. In Figure 8, the Arrhenius plots for the NO consumption rate on Cu/GP–Z(x) monoliths are compared to corresponding data on GP and Cu/GP monoliths, as well as on the reference Cu/Z powder. The domain of a kinetic regime is confirmed by the linear trend of the experimental data obtained for each catalyst in the low to moderate conversion range; however, when using bulk monolith samples, this corresponds to operation in a lower temperature range because of the correspondingly high mass of catalyst (low GHSV). In fact, SCR activity tests on the Cu/GP–Z(37) composite were also repeated using a fixed bed of powdered monolith catalyst obtained by grinding and sieving part of the original monolith. As shown in Figure 8, data points for the two sets of experiments ran at significantly different contact times collapsed into a single line after correction for the mass of catalyst, thus confirming that the reaction proceeded under kinetic control without significant mass transfer limitations, as was also the case in monolith catalysts.

In Table 3, the values of activation energy (E_a) are reported together with the kinetic constant for the NH_3-SCR of NO estimated at 150 °C. Cu/GP–Z(x) composite monoliths displayed an activation energy of 65–68 kJ mol^{-1}, which was equal to that evaluated for the reference Cu/Z powder catalyst, and compares with the value (61–75 kJ/mol) previously reported for Cu/ZSM5 self-sustained foam monoliths [10].

On the other hand, the estimated value of E_a on the Cu/GP monolith (49 kJ/mol) as well as its specific reaction rate were significantly lower, which points to a different reaction mechanism, in agreement with the different nature of the active copper species in this sample and to its negligible surface acidity. Due to the much higher specific activity of Cu sites when exchanged in the zeolite framework, the catalytic behaviour of Cu/Z prevailed on that of Cu/GP, even when the fraction of the zeolite in the composite monoliths was rather low, as well as when the Cu/Z was mechanically mixed with Cu/GP. However, the specific reaction rate calculated for the Cu/GP+Cu/Z mechanical mixtures was systematically lower than that of their corresponding composite monolithic samples, which agrees well with the lower surface acidity measured by NH_3-TPD.
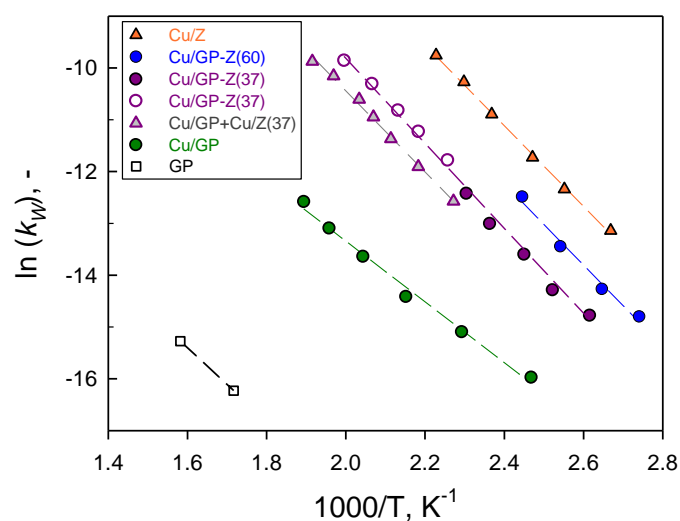
Figure 8. Arrhenius plots for the NO consumption rate per gram of catalyst during the NH$_3$-SCR of NO on pure Cu/GP and composite Cu/GP-Z(x) monoliths and reference (powder) catalysts.

A direct comparison of the specific SCR rate at 150 °C on Cu/GP–Z(x) monoliths vs. pure Cu/ZSM5 self-sustained foam monoliths [10] confirms that a better reactivity can be achieved on a mass basis in spite of their lower zeolite content, thus highlighting the promoting effect of the hierarchical structure associated to the simultaneous presence of a macro/meso/micro porosity in the case of GP–Z composites. However, the measured activity of Cu/GP–Z(x) is still somewhat lower than expected in comparison to the reference Cu/Z powder, probably due to the lower degree of copper exchange achieved during the ion exchange step with preformed monoliths, which remains the main drawback in the preparation of structured zeolite catalysts [10]. On the other hand, it can be argued that a synthesis scheme with inverted steps, i.e., introduction of pre-exchanged ZSM5 into the printable ink, entails risks of the possible loss of copper due to reverse exchange with sodium from the GP precursor.

3. Materials and Methods

3.1. Catalysts Preparation

Monoliths of Na-based GP, with circular section (diameter = 18 mm; height = 10–20 mm; Figure 1a) were manufactured by DIW as described in [32]. The GP slurry (ink) was prepared by mixing metakaolin, as an aluminosilicate source, and an activating solution composed of sodium silicate (SS2942, Ingessil S.r.l., Montorio, Italy), sodium hydroxide NaOH (Sigma–Aldrich, Steinheim, Germany) and distilled water. The SiO$_2$/Al$_2$O$_3$, Na$_2$O/Al$_2$O$_3$ and H$_2$O/Al$_2$O$_3$ ratios were 1.8, 1 and 25, respectively.

A commercial ZSM5 powder with a SiO$_2$/Al$_2$O$_3$ ratio = 23 was supplied by Zeolyst in its ammonium form: it was preliminarily treated for 2 h at 550 °C in air to obtain the corresponding H-form, before adding it to the ink as a filler. Na-bentonite (Sigma–Aldrich, Steinheim, Germany) and methylcellulose (Sigma–Aldrich, Steinheim, Germany) were added as rheological agents in order to obtain a printable ink. Distilled water was used to adjust the viscosity of the ink after the filler addition. The composition of the GP ink is reported in [32] whilst the nominal ZSM5 load in the zeolite-containing monoliths was either 37 or 60 wt% (dry basis). The printer (Delta 2040 Turbo, Wasproject, Massa Lombarda, Italy) was configured with a print speed of 10 mm/s and ink flow as needed to obtain constant extrusion through an 840 μm nozzle. The process was carried out at room temperature and in air. After printing the first layer, the nozzle was raised by 600 μm in the z-direction to print the next layer, in order to provide greater contact between the layers through their overlap. The first layer was composed of filaments parallel to each other, while the second layer was comprised of parallel filaments with a rotation of 90°

with respect to the previous layer; the subsequent layers followed the same arrangement. The printing process was repeated for 16 layers until the final dimensions of the lattice were reached. After printing, the samples were closed in a sealed plastic box and, considering the high amount of zeolites present in the samples, they were heat-treated at a mild temperature to avoid cracks during the geopolymerization as a result of differential shrinkage; the first step was carried out at room temperature for 1 day, then at 40 °C for 3 days, and finally at 75 °C for 1 day to complete the geopolymerization reaction.

Before ion exchange, all samples were treated in a 0.05 M HNO_3 acid solution for about 12 h to remove soluble species inhibiting ion exchange [32]. This treatment, as described in [32], caused the dissolution of alkaline sodium compounds deriving from the preparation of the GP, which otherwise would induce a high pH value (9–10) in the exchange metal solution, causing a rapid precipitation of $Cu(OH)_2$ on the outer shell of the monoliths. Copper exchange was carried out for 2 h using a 0.02 M $CuAc_2$ solution and a zeolite/solution ratio equal to 8 g/L, as reported in [8]. A ratio of 8 g GP/L was used for ion exchange of a pure GP monolith used as a reference sample for the SCR tests. After the ion exchange, all samples were washed twice with bi-distilled water, dried overnight in a stove at 120 °C and finally calcined at 400 °C under static air for 2 h.

Composite catalysts were labelled as Cu/GP–Z(x), where x corresponds to the weight content of ZSM5 (Z) in the sample.

3.2. Catalyst Characterization

SEM analysis was carried out on acid-treated monoliths using a FEI Inspect scanning electron microscope (SEM).

X-ray diffraction patterns were recorded on ground samples using a Philips X'Pert PRO apparatus with a working CuKα radiation and an anti-scatter silt width of 7.5 mm.

Compressive strength of acid-treated monoliths was evaluated at room temperature with a universal testing machine (Quasar 25, Galdabini 1890, Italy), with a constant crosshead speed of 0.5 mm/min. At least 10 samples for each composition were tested.

Copper content was determined by ICP–MS analysis using an Agilent 7500 ICP–MS instrument, after microwave-assisted digestion of samples.

Specific surface area measurements and micro/meso-pore analysis were performed in an Autosorb 1-C (Quantachrome) through N_2 adsorption at 77 K after degassing the samples for 2 h at 150 °C. The specific surface area and the pore size distribution were evaluated by the BET and NLDFT methods, respectively.

H_2-TPR analysis was carried out with a Micromeritics AutoChem 2020 equipped with a TC detector. Catalyst samples (150 mg) were pre-treated in-situ under air flow at 400 °C for 1 h; thereafter, 2 vol%. H_2/Ar mixture (50 cm^3 min^{-1}) was passed through the sample, heating from room temperature up to 700 °C at 10 °C min^{-1}.

3.3. NH₃-SCR Tests

The catalytic tests were carried out in a lab-scale rig already described in [10], consisting of a tubular quartz reactor (inner diameter = 20 mm) externally heated by a coaxial tubular furnace. Catalytic monoliths (d = 18 mm, l = 20 mm, average weight = 1.7 g) were wrapped with a ceramic tape to hold them in the reactor while avoiding any lateral gas by-pass. The inlet gas feed (composition: NO = NH_3 = 400 ppmv (NO_2 impurity < 4 ppmv), 6% O_2, He balance; total flow rate F = 25 Sdm^3 h^{-1}) was obtained by mixing gas streams from high purity cylinders (NO in He, NH_3 in He, O_2, He) regulated by independent mass flow controllers (BROOKS MFC SLA5850S). The GHSV (Gas Hourly Space Velocity) was 1.10^{-4} h^{-1} for all monoliths. The operating temperature ranged from 70 to 550 °C.

Analysis of reactants and products was performed by two continuous analyzers with independent detectors respectively for: (i) NH_3 (Tunable Diode Laser Sepctroscopy, GAS 3000R Geit-Europe); (ii) NO, N_2O (ND-IR) and NO_2 (UV; Emerson X-Stream XEGP). Water and NH_3 from the gas stream were removed using a Sycapent™ (P_2O_5) trap before entering the NO_x analyzer. N_2 concentration in the products was estimated by a N-balance

(assuming that N_2 was the only undetected N-bearing specie). NO/NH_3 conversion and N_2 selectivity were calculated according to [47]:

$$NO \text{ conversion } (\%) = \frac{[NO]_{in} - [NO]_{out}}{[NO]_{in}} \times 100$$

$$NH_3 \text{ conversion } (\%) = \frac{[NH_3]_{in} - [NH_3]_{out}}{[NH_3]_{in}} \times 100$$

$$N_2 \text{ selectivity } (\%) = \frac{[N_2]_{in} - [N_2]_{out}}{[N_2]_{in}} \times 100$$

The kinetic constant for the NO consumption rate and the corresponding apparent activation energy were estimated from integral reactor conversion data under the common assumptions of an ideal isothermal plug flow behaviour and a first-order dependency on NO concentration [10].

The activity tests were also repeated using a packed bed of powdered catalysts (0.125 g, obtained by grounding and sieving the monoliths in the size range 125–250 μm) under the same feed conditions, but at a shorter contact time (by a factor ~14). The same tests were performed using a mechanical mixture of Cu/GP (powdered) and Cu/Z to explore the possible effects of a closer interaction between the GP matrix and the zeolite phases in the printable ink used to produce the monoliths.

3.4. NH_3-TPD

Ammonia temperature programmed desorption tests were performed in the same experimental rig used for catalytic tests. Adsorption was performed by flowing (20 $Sdm^3\ h^{-1}$) 500 ppmv NH_3/He mixture at 100 °C over 0.100 g of ground monolith catalysts pretreated in air at 550 °C, as well as on mechanical mixtures of Cu/Z and Cu/GP powders having the same nominal compositions. When the initial NH_3 concentration was recovered, the sample was purged with He and thermal desorption was induced by ramping up the temperature from 100 to 650 °C at 10 °C/min under pure He flow (20 $Sdm^3\ h^{-1}$).

4. Conclusions

Geopolymer-based monoliths were produced by an additive manufacturing method (direct ink writing) with the introduction of up to 60% by weight of a pre-synthetized ZSM5 into the extrusion ink. Following a preliminary acid treatment to dissolve basic residues, monolithic samples were ion-exchanged with copper, aiming to obtain structured catalysts with a hierarchical texture and satisfactory mechanical resistance that can be potentially used for the NH_3-SCR of nitrogen oxides in industrial applications.

The textural, morphological and chemical characterization revealed that the main features of the Cu/ZSM5 catalytic fraction can be largely preserved when coupled to the geopolymer matrix to form composite monoliths. In particular, copper is preferentially located at the typical exchange sites in the zeolitic structure, whereas the formation of extra-framework CuO, detected for the pure geopolymer monolith, is minimized in the composites. A limited but measurable reduction in the surface activity of the zeolite fraction is observed for the composite materials, due to some poisoning effect of the strong acid sites caused by residual alkaline species in the geopolymer, which, on its own, has negligible ammonia adsorption capacity. Indeed, pure Cu/GP monoliths provided only poor SCR activity and low selectivity to N_2. On the other hand, the catalytic properties of the Cu/ZSM5 fraction towards the SCR prevail in the composite monoliths, thus providing a high NO conversion and a remarkable selectivity to N_2 over a wide range of temperatures. A direct comparison of activity data with a reference pure Cu/ZSM5 self-sustained foam monolith catalyst previously tested under similar conditions indicated a significant enhancement of the performance of the geopolymer–zeolite composites, which appear to benefit from their hierarchical structure given by the simultaneous presence of macro/mesoporous (geopolymer) and microporous (zeolite) phases. Although copper

exchange conditions should be optimized to further enhance the active phase loading while reducing the amount of residual (poisoning) alkaline species, those catalytic and mechanical features of the composite monoliths pave the way to novel developments for industrial SCR applications.

References

1. Zhang, W.; Qi, S.; Pantaleo, G.; Liotta, L.F. WO_3-V_2O_5 active oxides for NOx SCR by NH_3: Preparation methods, catalysts' composition, and deactivation mechanism-A review. *Catalysts* **2019**, *9*, 527. [CrossRef]
2. Zhang, J.; Li, X.; Chen, P.; Zhu, B. Research status and prospect on vanadium-based catalysts for NH3-SCR denitration. *Materials* **2018**, *11*, 1632. [CrossRef] [PubMed]
3. Tamilselvan, P.; Nallusamy, N.; Rajkumar, S. A comprehensive review on performance, combustion and emission characteristics of biodiesel fuelled diesel engines. *Renew Sustain. Energy Rev.* **2017**, *79*, 1134–1159. [CrossRef]
4. Mohan, S.; Dinesha, P.; Kumar, S. NOx reduction behaviour in copper zeolite catalysts for ammonia SCR systems: A review. *Chem. Eng. J.* **2020**, *384*, 123253. [CrossRef]
5. Namchot, W.; Jitkarnka, S. Upgrading of waste tyre-derived oil from waste tyre pyrolysis over Ni catalyst supported on HZSM5 zeolite. *Chem. Eng. Trans.* **2015**, *45*, 775–780.
6. Hamoud, H.I.; Valtchev, V.; Daturi, M. Selective catalytic reduction of NOx over Cu- and Fe-exchanged zeolites and their mechanical mixture. *Appl. Catal. B Environ.* **2019**, *250*, 419–428. [CrossRef]
7. Martín, N.; Vennestrøm, P.N.R.; Thøgersen, J.R.; Moliner, M.; Corma, A. Fe-Containing Zeolites for NH_3-SCR of NOx: Effect of Structure, Synthesis Procedure, and Chemical Composition on Catalytic Performance and Stability. *Chem. A Eur. J.* **2017**, *23*, 13404–13414. [CrossRef]
8. Lisi, L.; Pirone, R.; Russo, G.; Stanzione, V. Cu-ZSM5 based monolith reactors for NO decomposition. *Chem. Eng. J.* **2009**, *154*, 341–347. [CrossRef]
9. Nova, I.; Bounechada, D.; Maestri, R.; Tronconi, E.; Heibel, A.K.; Collins, T.A.; Boger, T. Influence of the substrate properties on the performances of NH_3-SCR monolithic catalysts for the aftertreatment of diesel exhaust: An experimental and modeling study. *Ind. Eng. Chem. Res.* **2011**, *50*, 299–309. [CrossRef]
10. Gargiulo, N.; Caputo, D.; Totarella, G.; Lisi, L.; Cimino, S. Me-ZSM5 monolith foams for the NH_3-SCR of NO. *Catal. Today* **2018**, *304*, 112–118. [CrossRef]
11. Peng, C.; Yan, R.; Peng, H.; Mi, Y.; Liang, J.; Liu, W.; Wang, X.; Song, G.; Wu, P.; Liu, F. One-pot synthesis of layered mesoporous ZSM5 plus Cu ion-exchange: Enhanced NH_3-SCR performance on Cu-ZSM5 with hierarchical pore structures. *J. Hazard. Mater.* **2020**, *385*, 121593. [CrossRef]
12. Sarno, M.; Scudieri, C. H_2 production improvement during pyrolysis catalyzed by zeolites. *Chem. Eng. Trans.* **2018**, *65*, 157–162.
13. Davis, M.E. Ordered porous materials for emerging applications. *Nature* **2002**, *417*, 813–821. [CrossRef] [PubMed]
14. Colombo, P.; Degischer, H.P. Highly porous metals and ceramics. *Mater. Sci. Technol.* **2010**, *26*, 1145–1158. [CrossRef]
15. Colombo, P.; Vakifahmetoglu, C.; Costacurta, S. Fabrication of ceramic components with hierarchical porosity. *J. Mater. Sci.* **2010**, *45*, 5425–5455. [CrossRef]
16. Tian, Q.; Sasaki, K. Structural characterizations of fly ash-based geopolymer after adsorption of various metal ions. *Environ. Technol.* **2021**, *42*, 941–951. [CrossRef]
17. dos Santos, L.K.; Botti, R.F.; de Mello Innocentini, M.D.; Marques, R.F.C.; Colombo, P.; de Paula, A.V.; Flumignan, D.L. 3D printed geopolymer: An efficient support for immobilization of Candida rugosa lipase. *Chem. Eng. Sci.* **2021**, *414*, 128843. [CrossRef]
18. Petlitckaia, S.; Barré, Y.; Piallat, T.; Grauby, O.; Ferry, D.; Poulesquen, A. Functionalized geopolymer foams for cesium removal from liquid nuclear waste. *J. Clean. Prod.* **2020**, *269*, 122400. [CrossRef]

19. Luukkonen, T.; Sarkkinen, M.; Kemppainen, K.; Rämö, J.; Lassi, U. Metakaolin geopolymer characterization and application for ammonium removal from model solutions and landfill leachate. *Appl. Clay Sci.* **2016**, *119*, 266–276. [CrossRef]

20. Sazama, P.; Bortnovsky, O.; Dědeček, J.; Tvaržková, Z.; Sobalík, Z. Geopolymer based catalysts-new group of catalytic materials. *Catal. Today.* **2011**, *164*, 92–99. [CrossRef]

21. Chen, H.; Zhang, Y.J.; He, P.Y.; Li, C.J.; Liu, L.C. Facile synthesis of cost-effective iron enhanced hetero-structure activated carbon/geopolymer composite catalyst for NH$_3$-SCR: Insight into the role of iron species. *Appl. Catal. A Gen.* **2020**, *605*, 117804. [CrossRef]

22. Hu, M.; Zhu, X.; Long, F. Alkali-activated fly ash-based geopolymers with zeolite or bentonite as additives. *Cem. Concr. Compos.* **2009**, *31*, 762–768. [CrossRef]

23. Rożek, P.; Król, M.; Mozgawa, W. Geopolymer-zeolite composites: A review. *J. Clean. Prod.* **2019**, *230*, 557–579. [CrossRef]

24. Zhang, J.; He, Y.; Wang, Y.P.; Mao, J.; Cui, X.M. Synthesis of a self-supporting faujasite zeolite membrane using geopolymer gel for separation of alcohol/water mixture. *Mater. Lett.* **2014**, *116*, 167–170. [CrossRef]

25. He, Y.; Cui, X.M.; Liu, X.D.; Wang, Y.P.; Zhang, J.; Liu, K. Preparation of self-supporting NaA zeolite membranes using geopolymers. *J. Membr. Sci.* **2013**, *447*, 66–72. [CrossRef]

26. Villa, C.; Pecina, E.T.; Torres, R.; Gómez, L. Geopolymer synthesis using alkaline activation of natural zeolite. *Constr. Build. Mater.* **2010**, *24*, 2084–2090. [CrossRef]

27. Wang, D.; Liu, Z.; Wang, H.; Xie, Z.; Tang, Y. Shape-controlled synthesis of monolithic ZSM5 zeolite with hierarchical structure and mechanical stability. *Microporous Mesoporous Mater.* **2010**, *132*, 428–434. [CrossRef]

28. Li, C.J.; Zhang, Y.J.; Chen, H.; He, P.Y. Highly-effective production of renewable energy dimethyl ether over geopolymer-based ferrierite. *Fuel* **2021**, *293*, 120486. [CrossRef]

29. Papa, E.; Medri, V.; Amari, S.; Manaud, J.; Benito, P.; Vaccari, A.; Landi, E. Zeolite-geopolymer composite materials: Production and characterization. *J. Clean. Prod.* **2018**, *171*, 76–84. [CrossRef]

30. Zocca, A.; Colombo, P.; Gomes, C.M.; Guenster, J. Additive Manufacturing of Ceramics: Issues, potentialities and opportunities. *J. Am. Ceram. Soc.* **2015**, *98*, 1983–2001. [CrossRef]

31. Shahzad, A.; Lazoglu, I. Direct ink writing (DIW) of structural and functional ceramics: Recent achievements and future challenges. *Compos. Part B Eng.* **2021**, *225*, 109249. [CrossRef]

32. Cepollaro, E.M.; Cimino, S.; Lisi, L.; Botti, R.; Colombo, P.; Franchin, G. Cu-exchanged 3D-printed geopolymer/ZSM5 monolith for selective catalytic reduction of NOx. *Chem. Eng. Trans.* **2021**, *84*, 67–72.

33. Huang, K.; Elsayed, H.; Franchin, G.; Colombo, P. Additive Manufacturing of SiOC scaffolds with tunable structure-performance relationship. *J. Eur. Ceram. Soc.* **2021**, *41*, 7552–7559. [CrossRef]

34. Al-Ketan, O.; Pelanconi, M.; Ortona, A.; Abu Al-Rub, R.K. Additive manufacturing of architected catalytic ceramic substrates based on triply periodic minimal surfaces. *J. Am. Ceram. Soc.* **2019**, *102*, 6176–6193. [CrossRef]

35. Skorina, T. Ion exchange in amorphous alkali-activated aluminosilicates: Potassium based geopolymers. *Appl. Clay Sci.* **2014**, *87*, 205–211. [CrossRef]

36. Uehara, M.; Sato, T.; Yamazaki, A. Suppression of Alkali Silica Reaction Using H+-type Geopolymer. *Q. Rep. RTRI.* **2018**, *59*, 90–96. [CrossRef]

37. Bortnovsky, O.; Dědeček, J.; Tvarůžková, Z.; Sobalík, Z.; Šubrt, J. Metal ions as probes for characterization of geopolymer materials. *J. Am. Ceram. Soc.* **2008**, *91*, 3052–3057. [CrossRef]

38. Davidovits, J. Geopolymers–Inorganic Polymer New Materials. *J. Therm. Anal.* **1991**, *37*, 1633–1656. [CrossRef]

39. Bakharev, T. Resistance of geopolymer materials to acid attack. *Cem. Concr. Res.* **2005**, *35*, 658–670. [CrossRef]

40. Kim, B.; Lee, S. Review on characteristics of metakaolin-based geopolymer and fast setting. *J. Korean Ceram. Soc.* **2020**, *57*, 368–377. [CrossRef]

41. He, P.; Fu, S.; Yuan, J.; Rao, J.; Xu, J.; Wang, P.; Jia, D. Celsian formation from barium-exchanged geopolymer precursor: Thermal evolution. *J. Eur. Ceram. Soc.* **2017**, *37*, 4179–4185. [CrossRef]

42. Allahverdi, A.; Skvara, F. Sulfuric acid attack on hardened paste of geopolymer cements—Part 1. Mechanism of corrosion at relatively high concentrations. *Ceram. Silik.* **2005**, *49*, 225–229.

43. Allahverdi, A.; Skvara, F. Sulfuric acid attack on hardened paste of geopolymer cements—Part 2. Corrosion mechanism at mild and relatively low concentrations. *Ceram. Silik.* **2006**, *50*, 1–4.

44. Ma, T.; Imai, H.; Yamawaki, M.; Terasaka, K.; Li, X. Selective Synthesis of Gasoline-Ranged Hydrocarbons from Syngas over Hybrid Catalyst Consisting of Metal-Loaded ZSM5 Coupled with Copper-Zinc Oxide. *Catalysts* **2014**, *4*, 116–128. [CrossRef]

45. Wang, H.; Jia, J.; Liu, S.; Chen, H.; Wei, Y.; Wang, Z.; Zheng, L.; Wang, Z.; Zhang, R. Highly efficient NO abatement over Cu-ZSM5 with special nanosheet features. *Environ. Sci. Technol.* **2021**, *55*, 5422–5434. [CrossRef] [PubMed]

46. Saha, B.; Vedachalam, S.; Dalai, A.K. Performance of geopolymer as adsorbent on desulphurization of heavy gas oil. *Can. J. Chem. Eng.* **2021**, 18. [CrossRef]

47. Cimino, S.; Totarella, G.; Tortorelli, M.; Lisi, L. Combined poisoning effect of K$^+$ and its counter-ion (Cl$^-$ or NO$_3^-$) on MnOx/TiO$_2$ catalyst during the low temperature NH$_3$-SCR of NO. *Chem. Eng. J.* **2017**, *330*, 92–101. [CrossRef]